

## Phonons in narrow carbon nanotubes

Ivanka Milošević,\* Edib Dobardžić, and Milan Damnjanović

Faculty of Physics, University of Belgrade, P. O. Box 368, Belgrade 11001, Serbia and Montenegro

(Received 17 August 2004; published 9 August 2005)

Accurate calculations of the phonon dispersion relations, phonon density of states, and phonon eigenvectors of the narrow single-wall carbon nanotubes in optimized geometry are carried out. The method applied is based on the force constants for graphene which reflect the long-range character of the dynamical matrix. Further, the relaxation and symmetry imposed modifications of the force constants are performed and the calculations are carried out by means of the fully symmetry implemented *POLSym* code. Shortcomings of the widely used frozen phonon model are overcome. The results obtained are compared to the Raman scattering measurements on the zeolite-grown nanotubes.

DOI: 10.1103/PhysRevB.72.085426

PACS number(s): 61.46.+w, 78.66.-w, 02.20.-a

### I. INTRODUCTION

Existence of the ultrasmall radius carbon nanotubes has been predicted<sup>1</sup> soon after the discovery of the standard diameter ones.<sup>2</sup> Quite recently, local density functional results<sup>3</sup> showed that the single-wall carbon nanotubes (SWCNTs) as thin as 3.42 Å are energetically stable implying that the zeolite-grown SWCNTs,<sup>4,5</sup> when exposed into the free space could persist. By high resolution transmission electron microscopy,<sup>6,7</sup> the diameter of the tubes encapsulated inside the hexagonally arrayed open channels of the zeolite AFI crystal was determined to be about the size of C<sub>20</sub>, the smallest fullerene. The tubes were further characterized through the optical absorption,<sup>6</sup> polarized Raman scattering,<sup>4,8–10</sup> diffuse x-ray scattering,<sup>11</sup> and electrical transport measurements.<sup>4,12</sup> More recently, systematic resonant Raman scattering study of the SWCNTs inside the AFI crystal using several laser lines has been performed<sup>10,13</sup> and the influence of the zeolite framework on the embedded SWCNTs (the zig-zag ones, in particular) has been calculated.<sup>14</sup> On the other hand, to the best knowledge of the authors, no thorough theoretical investigations of the phonon modes in narrow SWCNTs have been performed. For the tubes (5,0), (4,2) and (3,3) the radial breathing mode (RBM) frequencies have been calculated by a frozen phonon method<sup>15,16</sup> and their phonon density of states (PDOS) has been determined by a tight-binding molecular dynamics method.<sup>10,17</sup> More recently, *ab initio* density functional calculations of the phonon dispersions and PDOS for the tubes (5,0) and (4,2) have been carried out.<sup>13</sup>

In this paper we present an extensive and detailed theoretical study of the vibrational properties of the relaxed SWCNTs with diameters between 3.4 Å and 5 Å. Particular attention is paid to the 4-Å-diameter tubes where we compare our theoretical results to the recently reported Raman scattering measurements on the zeolite-grown nanotubes.<sup>10,13</sup>

The symmetry-based force constant method is applied: we fit the force constants to the recently reported<sup>18</sup> inelastic x-ray scattering measurements of the phonon dispersions of graphite and take into account the long-range character of the dynamical matrix.

Further, we modify the fitted force constants to the slightly strained sheet in order to match the equilibrium geometries<sup>3</sup> of the unfolded tubes and then additionally

kinematically<sup>19</sup> adjust them to the cylindrical web geometry. We use the *POLSym* simulation package,<sup>20</sup> based on the modified group projector technique<sup>21</sup> and line group symmetry<sup>22</sup> (for details on the method, see Ref. 19).

### II. SYMMETRY

Due to the one-to-one correspondence between the symmetry transformations and the atoms in the cylindrical web of a SWCNT the symmetry is essential for understanding underlying physical properties. All the symmetry transformations of a SWCNT form a monoperoic discrete infinite group, called line group<sup>23</sup> which is generated by three (in a case of the chiral tubes) or four (for armchair and zig-zag tubes) symmetry transformations.

Helical symmetry of the  $(n_1, n_2)$  tube is generated by a rotation of  $2r\pi/q$  around the tube axis followed by a translation for  $na/q$ , where  $a$  is a translational period of the tube and  $n$  is the greatest common divisor of  $n_1$  and  $n_2$ , while the parameters  $q$  and  $r$  are more complicated functions of  $n_1$  and  $n_2$  (for details see Ref. 22). The helical group thus obtained is denoted by  $\mathbf{T}_q^r(a)$ . The remaining two generators are rotation for  $2\pi/n$  around the vertical axis (i.e., tube axis) and twofold rotation  $U$  around the horizontal axis. Hence, generally, the full symmetry group of a chiral tube is a product of the helical subgroup  $\mathbf{T}_q^r(a)$  and the point subgroup  $\mathbf{D}_n$ . Analogously, for the achiral tubes,  $(n, 0)$  and  $(n, n)$ , their symmetry groups are product of  $\mathbf{T}_{q=2n}^{r=1}(a)$  and  $\mathbf{D}_{nh}$ , as there is a vertical mirror symmetry  $\sigma_v$  as well. All these groups are nonsymmorphic,<sup>22</sup> i.e., the corresponding isogonal point groups,  $\mathbf{D}_q$  and  $\mathbf{D}_{2nh}$ , are not subgroups.

The parameters  $q$ ,  $r$  and  $n$ , which determine full symmetry (as well as the isogonal point group) of the narrow tubes considered here are given in Table I. From the above factorization of the SWCNTs symmetry groups it is easy to see that the corresponding irreducible representations (IRs) are one- and two-dimensional in the case of the chiral tubes while one-, two- and four-dimensional for the achiral ones.

Apart from the parities two types of quantum numbers are used: rototranslational and helical.<sup>24,25</sup> The former, consisting of linear momenta  $k$  and total angular momenta  $m$  are not conserved in Umklapp processes. While  $k$  is the conserved linear quasimomentum (canonically conjugated to the dis-

TABLE I. Symmetry parameters of the narrow SWCNTs.

$(n_1, n_2)$	(4,0)	(3,2)	(4,1)	(5,0)	(3,3)	(4,2)	(5,1)	(6,0)	(4,3)	(5,2)
$q$	8	38	14	10	6	28	62	12	74	26
$r$	1	15	11	1	1	9	51	1	21	11
$n$	4	1	1	5	3	2	1	6	1	1

crete translations), the angular momentum  $m$  is not, as it appears due to the isogonal rotations being not the elements of the total symmetry group. In contrast, the helical quantum numbers, i.e., helical momenta  $\tilde{k}$  and complementary angular momenta  $\tilde{m}$ , are always conserved since  $\tilde{k}$  is conjugated to the helix  $\mathbf{T}_q^r(a)$  (thus combining angular and linear momenta) while  $\tilde{m}$  is related to the rotations of the point subgroups  $\mathbf{D}_n$  or  $\mathbf{D}_{nh}$ .

Each IR can be labeled by either set of quantum numbers:  $(k, m)$  and  $(\tilde{k}, \tilde{m})$ . For fixed  $m$  and  $k$  allowed over the irreducible domain (ID)  $[0, \pi/a]$  of the Brillouin zone (BZ) one gets the  $m$  series. Likewise, the  $\tilde{m}$  series is obtained for fixed  $\tilde{m}$  and  $\tilde{k}$  running over the ID  $[0, \pi q/na]$  of the helical BZ. Altogether the number of the  $m$  and  $\tilde{m}$  series is  $q$  and  $n$ , respectively. Consequently, the  $\tilde{k}\tilde{m}$  quantum numbers are more practical when phonon (or electron<sup>24</sup>) dispersions in the chiral tubes are considered (and graphically presented) as these tubes are usually characterized by a large  $q$  value (due to the large number of atoms within the unit cell). Anyway, by means of the transition rules<sup>25</sup> it is easy to switch between the two sets of the quantum numbers.

Concerning the parities, the ones with respect to the  $z$ -reversal symmetries ( $U$  or  $\sigma_h$ ) are denoted by  $+$  or  $-$  while  $A$  and  $B$  respectively indicate even and odd character of the parity which is due to the vertical mirror symmetry.

### III. RAMAN ACTIVE MODES

Resonant Raman scattering has proved to provide a reliable tool for characterizing SWCNTs. However, out of 15 (for the chiral tubes) and eight (for the achiral tubes) Raman active vibrational modes<sup>19,22,26</sup> only the radial breathing mode and the tangential G-band modes of vibration are strongly resonance enhanced<sup>29,30</sup> comprising the main features in first-order Raman spectra. While the low-frequency perfectly symmetric RBM has no counterpart in the graphene sheet the G-band high energy modes (HEMs) can be interpreted by splitting (due to the symmetry breaking after folding the sheet into the tube) of the  $E_{2g}$  peak in the Raman spectra of the 2D graphene sheet.

In what follows we focus firstly on the RBM, which in a case of the conventional SWCNTs has shown to be very useful for the identification of the tube diameter. Subsequently we turn to the inspection of the more complex Raman spectral feature: frequencies and atomic displacements of the G-band HEMs.

#### A. Radial modes of vibration

The breathing mode of vibration, in which all the atoms undergo an equal radial displacement, is a unique feature in

the SWCNTs Raman spectra. Being sensitive to the tube diameter it is widely used to characterize samples of SWCNTs. Many theoretical calculations<sup>17,19,28,29,31,32</sup> have shown that its frequency  $\omega_{\text{RBM}}$  decreases with the diameter  $D$  of the tube: e.g.,  $\omega_{\text{RBM}}[\text{cm}^{-1}] \approx 224.3/D[\text{nm}]$  (from Ref. 19). Being purely symmetric mode, it transforms according to the IR:  ${}_{0}A_0^+$  ( $A_{1g}$ , subscript “g” is for the achiral tubes only), where the line group (isogonal point group) notation is used. However, the radial breathing mode, in a case of the ultrathin nanotubes, is not quite radial as it appears to have finite components along and normal to the tube axis (tangential to the cylindrical surface). Namely, as the achiral tubes possess nontrivial stabilizer<sup>22</sup> (i.e., the carbon atoms sit in vertical and horizontal mirror planes, in zig-zag and armchair tubes, respectively) the RBM displacement has no circumferential component in the zig-zag tubes (due to the stabilizer that is generated by a vertical mirror plane), while in the armchair tubes (where the stabilizer is generated by a horizontal mirror plane) it does not have the longitudinal component. On the other hand, the chiral tubes have trivial stabilizer and no mirror symmetry<sup>22</sup> and their RBM displacement is thus allowed to have both the circumferential and the longitudinal component. As expected, the first one,  $\phi$ , increases, whereas the second one,  $z$ , decreases with the chiral angle  $\theta$ , Fig. 1. The contribution of these components to the RBM displacement amplitude decreases rapidly with the tube diameter  $D$ :

$$z(D, \theta)(\%) = \left( \frac{24}{D} + \frac{97}{D^3} \right) |\cos 3\theta|, \quad (1)$$

$$\phi(D, \theta)(\%) = - \left( \frac{26}{D} - \frac{4.1}{D^3} \right) |\sin 3\theta|, \quad (2)$$

where  $D$  should be inserted in the units of angstrom.

Since in the case of the narrow tubes the deviation from the radial direction is considerable, the generally used frozen phonon method<sup>15,32</sup> where the tube radius is simply increased and decreased by, e.g., 1% and 2%, when applied to the narrow nanotubes would somewhat overestimate the RBM frequency: from  $5 \text{ cm}^{-1}$  to  $12 \text{ cm}^{-1}$ . This error is chirality dependant (Fig. 2) and diminishes with the SWCNTs' diameter: it is about  $1.5 \text{ cm}^{-1}$  for the  $\sim 1.4$ -nm-diameter tubes. A fit to the inverse diameter gives the constant of proportionality which is somewhat larger than in a case of the standard diameter nanotubes<sup>19</sup> and no significant chirality dependence of the RBM frequency is obtained:

$$\omega_{\text{RBM}}(\text{cm}^{-1}) = \frac{259}{D(\text{nm})} - \frac{1.4}{D^3(\text{nm})}, \quad (3)$$

which contradicts recent frozen phonon model calculations.<sup>16</sup> Namely, within such an approach RBM is modeled as totally

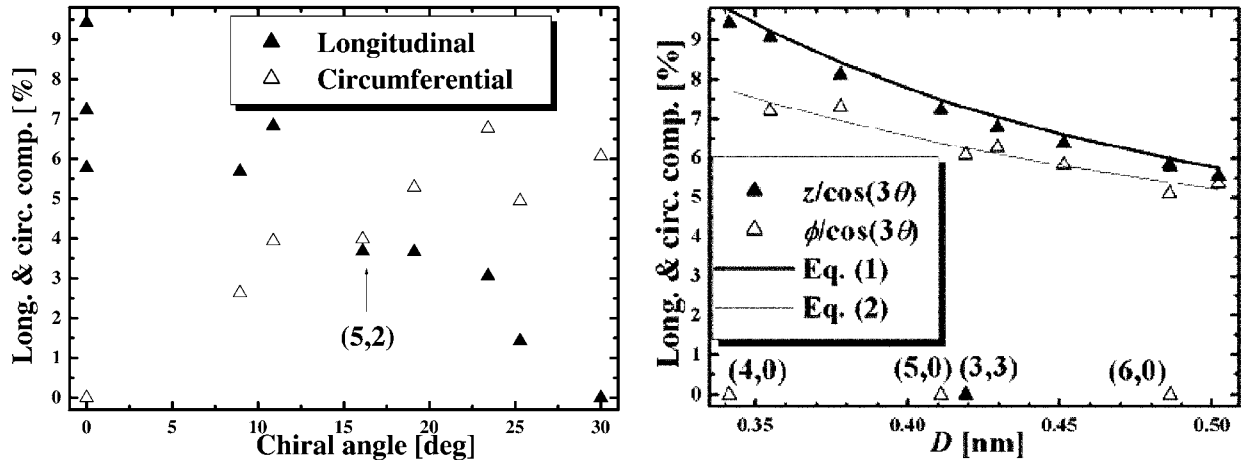


FIG. 1. RBM longitudinal,  $z$ , and circumferential,  $\phi$ , components. Left:  $z$  and  $\phi$  dependence on the chiral angle,  $\theta$ . Overlap of the longitudinal and circumferential values in a case of the (5,2) tube is indicated. Right:  $z/\cos 3\theta$  and  $\phi/\sin 3\theta$  as a function of tube diameter. Solid curves are fits (1) and (2).

radial displacement and consequently, the square root of the corresponding dynamical matrix element is interpreted as the RBM frequency. However, since RBM has finite nonradial components which are chirality sensitive, the RBM frequencies calculated within frozen phonon approximation reflect the chirality dependence of the RBM nonradial components.<sup>27</sup>

It is interesting to note that in SWCNTs there is also an exact radial mode of vibration. Using simple symmetry arguments existence of such a phonon mode can be easily deduced: The longitudinal translations change the sign upon the  $z$ -reversal symmetry while they are invariant under all the other symmetry transformations. Thus the corresponding acoustic mode transforms as the  ${}_0A_0^-(A_{2u})$  tensor. Further, in a case of the chiral tubes the twisting acoustic mode is of the same symmetry (it has to be odd with respect to the  $U$ -transformation) and the frequency number of the  ${}_0A_0^-$  in

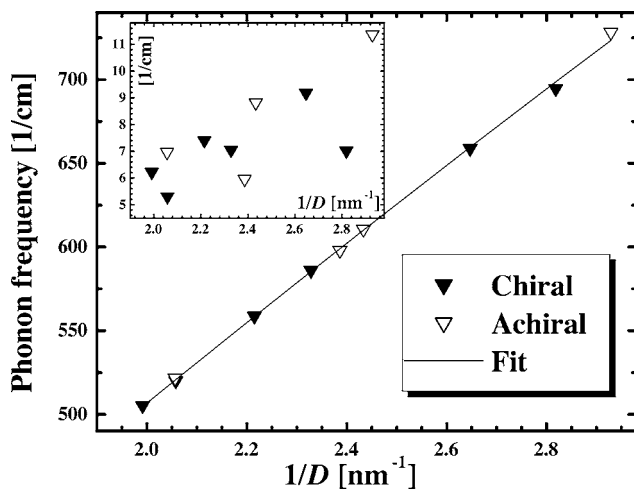


FIG. 2. RBM frequencies of the narrow SWCNTs as a function of the inverse diameter. Solid symbols are chiral tubes, open ones are achiral tubes; linear fit is given by Eq. (3). The inset shows the RBM frequency overestimation  $\Delta\omega$  which frozen phonon method gives.

the dynamical representation is three. Consequently, the third (optic)  ${}_0A_0^-$  mode is purely radial (as it has to be orthogonal onto both the longitudinal and the twisting mode of the same symmetry). On the other hand, in a case of the achiral tubes, where the extra mirror plane symmetries emerge, the twisting mode is to change the sign upon the reflection in the vertical mirror plane and it is to be invariant under the horizontal mirror plane transformation; hence it transforms as the  ${}_0B_0^+(A_{2g})$  tensor. Moreover, the dynamical representation of the zig-zag (armchair) tubes contains the  ${}_0A_0^-({}_0B_0^+)$  representation twice. Therefore the optic  ${}_0A_0^-({}_0B_0^+)$  mode should be orthogonal onto the  $z$  axis (the axis tangential to the tube circumference). As the  ${}_0A_0^-({}_0B_0^+)$  tensor is invariant under the reflection in the vertical (horizontal) mirror plane, the optical mode  ${}_0A_0^-({}_0B_0^+)$  is therefore exactly radial.

Hence, the exact radial mode, unlike the RBM, is not totally symmetric since the adjacent carbon atoms undergo an equal radial displacement but in the opposite directions. It is both infrared and Raman active in a case of the chiral tubes while only Raman and only infrared active for the armchair and zig-zag tubes, respectively.

## B. G-band modes

As established by resonant Raman scattering measurements and lattice dynamics calculations,<sup>29</sup> components of the G-band in the Raman spectra of achiral SWCNTs have  ${}_0A_0^+(A_{1g})$ ,  ${}_0E_1^-(E_{1g})$ ,  ${}_0E_2^+(E_{2g})$  symmetry while in a case of the chiral tubes there are six components, a pair of each having the following symmetries:  ${}_0A_0^+(A_1)$ ,  ${}_0E_1(E_1)$ ,  ${}_0E_2(E_2)$ .

Since the frequency number of the  ${}_0A_0^+$  in the dynamic representation of the achiral and chiral tube is two and three, respectively,<sup>22</sup> and since the RBM is totally symmetric, the HEM of vibration in the achiral tubes must take place in the plane which is orthogonal onto the radial breathing displacement vector. Similarly, in a case of the chiral tubes, the two HEMs of vibration form an orthogonal basis in such a plane. Bearing in mind that the symmetric displacement in the armchair or zig-zag tube cannot have longitudinal or circumfer-

ential component as the stabilizer contains horizontal or vertical mirror plane and that the RBM is only nearly radial, one deduces easily that the HEM in armchair or zig-zag tube is almost (but never exactly) circumferential or longitudinal. As in a case of the chiral tubes no such restriction occurs (due to the lack of the mirror symmetry) these tubes happen to have one (almost) circumferential and one (almost) longitudinal HEM. If the RBM was exactly radial these modes would determine the tangential plane to the tubule. Nevertheless, as the nonradial components of the RBM are vanishingly small for the larger tubes, the frequently used notion of the tangential fully symmetric mode within the G-band is fully justified. The notion appears to make sense also in a case of the narrow tubes since the declination from the both circumferential and longitudinal direction is at most  $3.8^\circ$  for the tube (5,2) which is fairly narrow and almost equally “distant” from both the zig-zag and armchair geometry (Fig. 1).

Unlike the symmetric HEM, the descriptive notion of the tangential modes of vibration does not hold for the doubly degenerate G-band phonons in the chiral tubes as the corresponding atomic displacements usually have substantial radial component as well. Namely, since the Hamiltonian is degenerated, the particular result obtained from the symmetry based calculations is specified by the (arbitrary) choice of the matrix forms of the corresponding IR, but any other (of infinitely many) equivalent representation(s) would yield the vectors from the same eigensubspace, connected to the previous ones by an orthogonal transformation. Further, as the range of the projector onto the corresponding IR ( ${}_0E_1$  or  ${}_0E_2$ ) is a six-dimensional real space<sup>22</sup> any atomic displacement direction is allowed. On the other hand, in a case of the methods not based on symmetry details of calculation single out the particular pair of eigenvectors. For instance, the exhaustive illustrations of the  $E_1$  and  $E_2$  modes in some of the chiral tubes<sup>33</sup> represent just one of infinitely many diverse possibilities.

In contrast to the chiral, the doubly degenerated HEMs of the achiral tubes are characterized by the sharp horizontal mirror parity ( ${}_0E_1^-$  is odd and  ${}_0E_2^+$  is even) which in a case of the armchair tubes severely restricts the possible directions of the corresponding atomic displacements. Since in these tubes the carbon atoms sit on the horizontal mirror planes (i.e., the stabilizer is  $C_{1h}$ ) the corresponding odd or even phonon modes are necessarily longitudinal or circumferential.<sup>29</sup> As the horizontal mirror plane does not pertain to the stabilizer of the zig-zag tubes both the  ${}_0E_1^-$  and  ${}_0E_2^+$  atomic displacements in these tubes may have finite circumferential and longitudinal components.

The calculated frequencies of the HEMs are shown in Fig. 3. The splitting of the two  ${}_0A_0^+(A_1)$  modes in the chiral tubes ranges between  $30\text{ cm}^{-1}$  and  $70\text{ cm}^{-1}$ , considerably less than the splitting obtained by extrapolating the empirical formula<sup>34</sup> defined for the tubes with diameters between 0.95 nm and 2.62 nm.

Generally, the order of the frequencies at the  $\Gamma$  point ( $k=0$ ) differs from the one expected in the simple zone folding approach [e.g., with decreasing frequency the branches are sorted as  $m=0, 0, 1, 1, 5, 2, 2, 3$  in a case of the (5,0) tube]. However, the ordering of the Raman active HEMs happen to match the zone folding prediction: Sorted by decreasing the

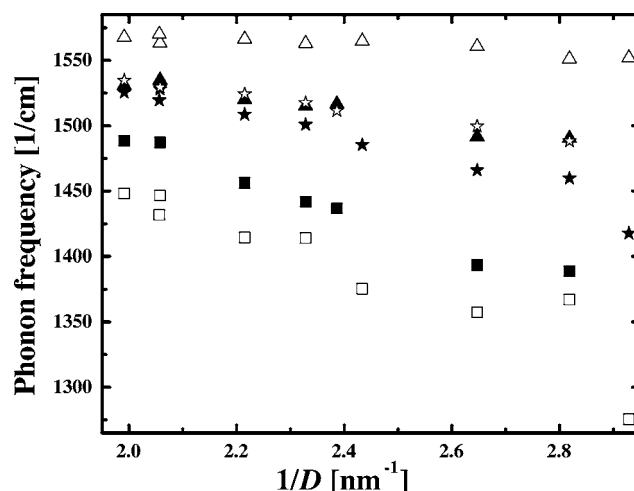


FIG. 3. Raman active HEM frequencies plotted as a function of the inverse radius. Triangles denote modes with  $A_1$  and  $A_{1g}$  symmetry, asterisks the ones with  $E_1$  and  $E_{1g}$  symmetry while the modes with  $E_2$  and  $E_{2g}$  symmetry are depicted as squares. Solid symbols are the circumferential modes, open ones are the longitudinal modes.

frequency it is  $A_{1g}$ ,  $E_{1g}$ ,  $E_{2g}$  for both the zig-zag and the armchair narrow tubes, unlike the case of the tubes with larger diameter.<sup>35</sup>

#### IV. 4-Å DIAMETER TUBES

Recently, porous aluminophosphate  $AlPO_4$  zeolite crystal was used as a template to grow monosized SWCNTs by pyrolyzing hydrocarbon molecules in its channels.<sup>4</sup> Under the assumption of the van der Waals type of interaction between the SWCNT inside the channel and the crystal the diameter of the SWCNT should be around 0.4 nm. Also, by high-resolution transmission electron microscopy the diameter of the zeolite-grown tubes was determined<sup>6</sup> to be  $0.42 \pm 0.02$  nm. Within this diameter range there are four different chiralities: (5,0), (3,3), (4,2), and (5,1). Diameter of the largest, (5,1), SWCNT in ideal cylindrical structure is 0.436 nm. Thus, it is expected to exceed the upper limit of 0.44 nm when relaxed in a free space. In a case of the zeolite-grown SWCNTs nanometer-sized channels must have an important function in their stabilization. Namely, although the narrow SWCNTs were predicted to be energetically stable<sup>2,3</sup> when exposed into a free space there are certain indications of their instability,<sup>4</sup> especially under electron-beam irradiation. Therefore we do not rule out the possibility (at least not on the diameter range basis) the (5,1) tube to be zeolite-grown.

It is not easy to determine accurately the chirality from electron microscopy. Raman spectroscopy seems to be a more helpful characterization tool. It is also sensitive to the concentration of the particular tube types and to the channels' filling rate. The interpretation of the Raman scattering measurements relies on calculated optical absorption and phonon dispersions. In the rest of the paper we present and discuss the latter for the above listed four 0.4-nm-sized tubes.

In Fig. 4 phonon dispersion of the achiral tubes are de-

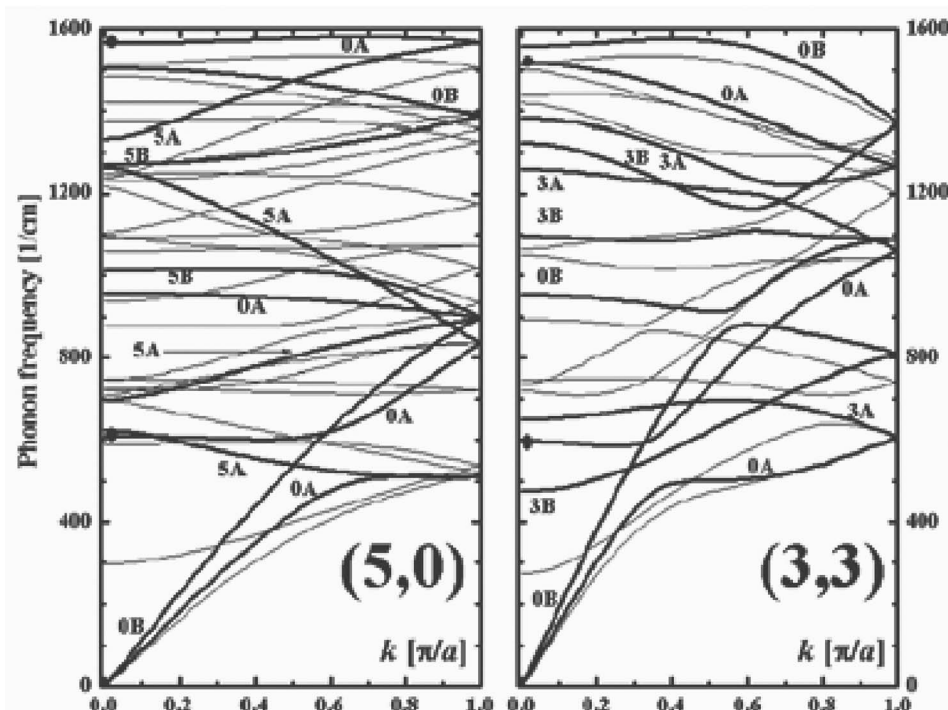


FIG. 4. Phonon dispersions of the (5,0) and (3,3) nanotubes given by  $km$  quantum numbers. The bands with  $m=0$  and  $m=n$  (bold lines) are double-degenerate, with the vertical mirror parity (even and odd is indicated by A and B). The remaining bands are fourfold degenerate. Circles denote the radial breathing and high energy totally symmetric modes.

pictured. Due to the relatively small  $q$  values the  $km$  representation is used. Out of the  $\Gamma$  point the branches with  $m=0$  and  $m=n$  are double degenerate and have well defined parity under vertical mirror reflection. All the other bands are fourfold degenerate. On the other hand, phonon branches of the (4,2) and (5,1) tubes are given by the helical  $\tilde{k}\tilde{m}$  quantum numbers (Fig. 5). The length of the BZ is  $14\pi/a$  and  $62\pi/a$ , respectively. The bands with  $\tilde{m}=0$  are given by the bold lines. A band with a given  $\tilde{m}$  can be understood as “unfolding” the bands in the  $km$  description by obeying the Umklapp rules<sup>25</sup> at the zone boundary. The frequencies extend up to

$1570 \text{ cm}^{-1}$ , similar to the recent density functional theory calculations.<sup>13</sup> All the phonon bands are double degenerate (apart from the modes at  $k=0$ ). Finally, the totally symmetric phonon modes (RBM and HEMs) which are observable by Raman spectroscopy are indicated in the figures.

For the relaxed (5,0), (3,3), (4,2), (5,1) tubes (the geometry parameters of the relaxed configurations are taken from Ref. 3) the calculated RBM frequencies are  $611 \text{ cm}^{-1}$ ,  $598 \text{ cm}^{-1}$ ,  $586 \text{ cm}^{-1}$ , and  $559 \text{ cm}^{-1}$ , respectively. The larger the diameter, the smaller RBM frequency (likewise the larger radius tubes)—in agreement with the quite recent calculations by Li *et al.*<sup>36</sup> and in contrast to the previously reported calculations<sup>13,15,37</sup> which give the following RBM frequency ordering (starting from the lowest one): (3,3), (4,2), (5,0). The results of ours are also in a qualitative agreement with

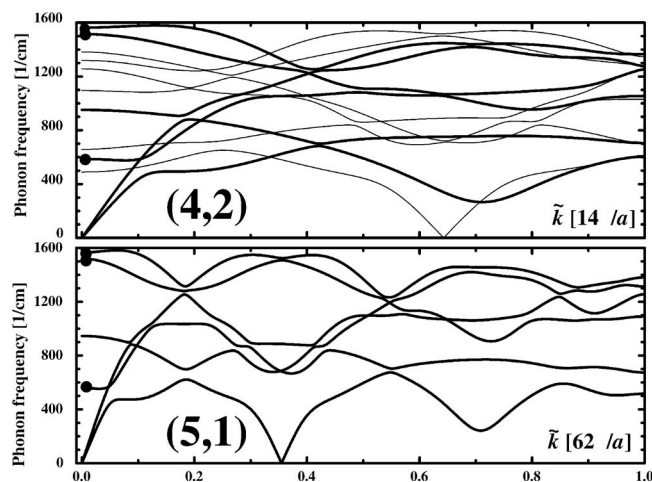


FIG. 5. Phonon dispersions of the (4,2) and (5,1) nanotubes given by  $\tilde{k}\tilde{m}$  quantum numbers. For (4,2) tube, as  $n=2$ , six bands are assigned by  $m=0$  (bold), and the other six by  $m=1$  (dashed), while for (5,1) there are only six  $m=0$  branches. All the bands are double degenerate. Circles denote the radial breathing mode and the high energy totally symmetric modes.

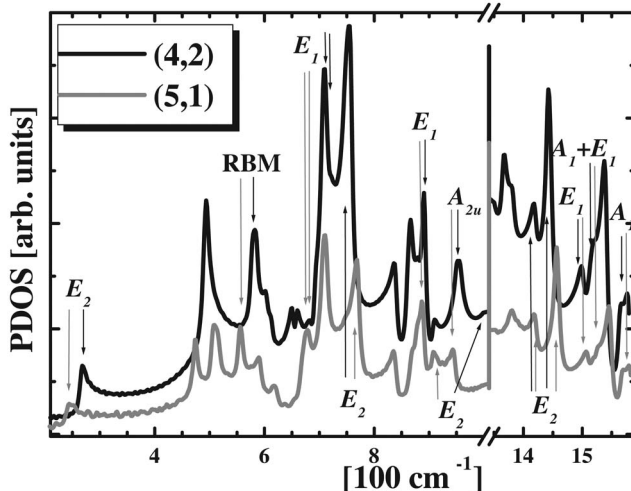


FIG. 6. PDOS of the (4,2) and (5,1) SWCNTs in low- and high-energy regions.

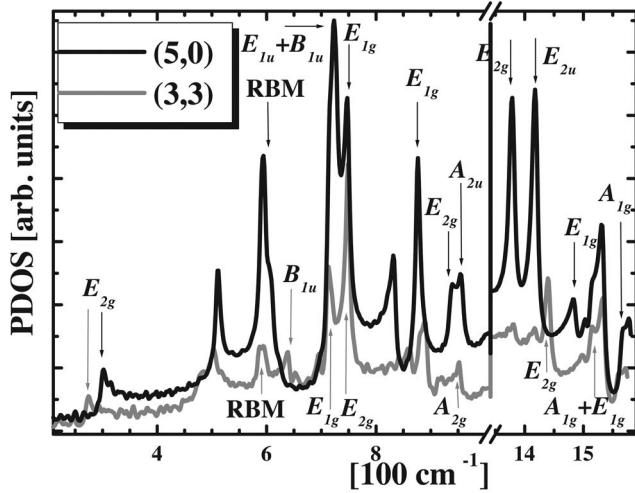


FIG. 7. PDOS of the (5,0) and (3,3) SWCNTs in low- and high-energy regions.

the measurements of Jorio and co-workers<sup>10</sup> and with the more recently reported Raman studies of the AFI-grown tubes.<sup>13,36</sup> The experimental values that have recently been reported in Ref. 37 are also matched. However, we ascribe the lower frequency to the (4,2) and the higher one to the (5,0) tube.

As the Raman active modes fall into two different energy regions we provide low-energy and high-energy phonon density of states (PDOS) plots for each of the tubes. While in a case of the chiral tubes (Fig. 6) all the peaks in the low-energy PDOS (apart from the one coming from the RBM) correspond to the Raman inactive phonon modes (i.e., with  $|m|$  larger than two) in a case of the achiral tubes besides the RBM peak there are features in the low-energy PDOS also coming from the Raman active modes:  ${}_0E_2^+(E_{2g})$  at  $350\text{ cm}^{-1}$  and  ${}_0E_1^-(E_{1g})$  at  $750\text{ cm}^{-1}$  for the (5,0) tube (Fig. 7). Therefore, the peak at  $390\text{ cm}^{-1}$ , in the experimentally obtained<sup>13</sup> low energy Raman spectra of SWCNTs embedded in a zeolite crystal can be ascribed to the Raman active  $E_{2g}$  mode of the (5,0) SWCNT. However, not only the Raman active modes are those which correspond to the PDOS peaks, as shown in Fig. 6 and Fig. 7.

The calculated frequencies of the G-band modes are given in Table II. The values are at most 3% lower than the measured ones.<sup>10,13</sup> The agreement is much better when the AFI crystal lattice constant is taken (instead of the free SWCNT unit cell length) indicating the role of the AFI template in the stabilization of the incased tubes. Also, the possible  $A_{1g}$  HEM softening, by a Peirels-like mechanism,<sup>38</sup> in the metallic, (3,3) and (5,0), tubes has not been taken into account.

Finally, it is interesting to note that the exactly radial mode shows a high density exhibiting thus well pronounced peak in the PDOS plot. The calculated frequency for the

TABLE II. Calculated frequencies of the Raman active high-energy modes.

SWCNT	IR	Frequency (cm <sup>-1</sup> )	SWCNT	IR	Frequency (cm <sup>-1</sup> )
(5,0)	$A_{1g}$	1565	(3,3)	$A_{1g}$	1517
	$E_{1g}$	1485		$E_{1g}$	1512
	$E_{2g}$	1375		$E_{2g}$	1437
(4,2)	$A_1$	1515	(5,1)	$A_1$	1520
		1563			1566
	$E_1$	1501		$E_1$	1509
		1517			1524
		1414			1414
$E_2$	1442	$E_2$	1456		

armchair (3,3) and the zig-zag (5,0) tubes are very close:  $954\text{ cm}^{-1}$  and  $958\text{ cm}^{-1}$ , respectively. However, the suitable measurement can distinguish between these two as in the first case the mode is Raman active, while in the latter it is infrared active. Concerning the chiral tubes, the modes are both Raman and infrared active and the frequencies are  $952\text{ cm}^{-1}$  for (4,2) and  $946\text{ cm}^{-1}$  for (5,1).

## V. CONCLUSION

In conclusion, we performed comprehensive theoretical study of the vibrational properties of the narrow SWCNTs, the 0.4-nm-sized ones in particular. The full-symmetry groups of the narrow tubes are determined and the phonon dispersions and atomic displacements are calculated within the specifically symmetry based force constants approach. Its direct output together with the frequencies and the displacements are the phonon branches assignment by the full set of the conserved quantum numbers, band degeneracy, Raman and infrared active modes. Further, PDOS is calculated and its main features are ascribed by Raman or infrared active modes. The eigenvectors of the phonon modes are calculated exactly and thus the shortcomings of the frozen phonon method are overcome. As a consequence, no significant chirality dependence of the RBM frequency is obtained and it is shown that the rule: “the lower the diameter the higher the RBM frequency” holds for the ultrathin SWCNTs as well. Finally, the results of the exhaustive symmetry-based numerical study presented here may help to resolve the ambiguities in the identification of the AFI-grown tubes.

## ACKNOWLEDGMENTS

We thank J. Maultzsch and C. Thomsen for helpful discussions and for the experimental data of the graphite phonon dispersions. This work was supported by Serbian Ministry of Science (project MNTR-1924) and Deutsche Forschungsgemeinschaft (project DFG 436 YUG 113/2/0-1).

- \*Electronic address: ivag@afrodita.rcub.bg.ac.yu; URL: <http://www.ff.bg.ac.yu/nanoscience>
- <sup>1</sup>S. Sawada and N. Hamada, *Solid State Commun.* **83**, 917 (1992).
  - <sup>2</sup>S. Iijima, *Nature (London)* **354**, 56 (1991).
  - <sup>3</sup>I. Cabria, W. Mintmire, and C. T. White, *Phys. Rev. B* **67**, 121406(R) (2003).
  - <sup>4</sup>Z. K. Tang, H. D. Sun, J. Wang, J. Chen, and G. Li, *Appl. Phys. Lett.* **73**, 2287 (1998).
  - <sup>5</sup>N. Wang, Z. K. Tang, G. D. Li, and J. S. Chen, *Nature (London)* **408**, 50 (2000).
  - <sup>6</sup>Z. M. Li, Z. K. Tang, H. J. Liu, N. Wang, C. T. Chan, R. Saito, S. Okada, G. D. Li, J. S. Chen, N. Nagasawa, and S. Tsuda, *Phys. Rev. Lett.* **87**, 127401 (2001).
  - <sup>7</sup>Y. F. Chan, H. Y. Peng, Z. K. Tang, and N. Wang, *Chem. Phys. Lett.* **369**, 541 (2003).
  - <sup>8</sup>G. D. Li, Z. K. Tang, N. Wang, and J. S. Chen, *Carbon* **40**, 917 (2002).
  - <sup>9</sup>H. D. Sun, Z. K. Tang, J. Chen, and G. Li, *Solid State Commun.* **109**, 365 (1999).
  - <sup>10</sup>A. Jorio, A. G. Souza Filho, G. Dresselhaus, M. S. Dresselhaus, A. Righi, F. M. Matinaga, M. S. S. Dantas, M. A. Pimenta, J. Mendes Filho, Z. M. Li, Z. K. Tang, and R. Saito, *Chem. Phys. Lett.* **351**, 27 (2002).
  - <sup>11</sup>P. Launois, R. Moret, D. Le Bolloch, P. A. Albouy, Z. K. Tang, G. Li, and J. Chen, *Solid State Commun.* **116**, 99 (2000).
  - <sup>12</sup>Z. K. Tang, H. D. Sun, and J. Wang, *Physica B* **279**, 200 (2000).
  - <sup>13</sup>M. Hulman, H. Kuzmany, O. Dubay, G. Kresse, L. Li, and Z. K. Tang, *J. Chem. Phys.* **119**, 3384 (2003).
  - <sup>14</sup>O. Dubay and G. Kresse, *Carbon* **42**, 979 (2004).
  - <sup>15</sup>H. J. Liu and C. T. Chan, *Phys. Rev. B* **66**, 115416 (2002).
  - <sup>16</sup>J. Kürti, V. Zólyomi, M. Kertesz, and G. Sun, *New J. Phys.* **5**, 125.1 (2003).
  - <sup>17</sup>R. Saito, T. Takeya, T. Kimura, G. Dresselhaus, and M. S. Dresselhaus, *Phys. Rev. B* **57**, 4145 (1998).
  - <sup>18</sup>J. Maultzsch, S. Reich, C. Thomsen, H. Requardt, and P. Ordejón, *Phys. Rev. Lett.* **92**, 075501 (2004).
  - <sup>19</sup>E. Dobardžić, I. Milošević, B. Nikolić, T. Vuković, and M. Damnjanović, *Phys. Rev. B* **68**, 045408 (2003).
  - <sup>20</sup>I. Milošević, A. Damnjanović, and M. Damnjanović, in *Quantum Mechanical Simulation Methods in Studying Biological Systems*, edited by D. Bicout and M. Field (Springer-Verlag, Berlin, 1996), Chap. XIV.
  - <sup>21</sup>M. Damnjanović, T. Vuković, and I. Milošević, *J. Phys. A* **33**, 6561 (2000).
  - <sup>22</sup>M. Damnjanović, I. Milošević, T. Vuković, and R. Sredanović, *Phys. Rev. B* **60**, 2728 (1999).
  - <sup>23</sup>I. Milošević and M. Damnjanović, *Phys. Rev. B* **47**, 7805 (1993).
  - <sup>24</sup>C. T. White, D. H. Robertson, and J. W. Mintmire, *Phys. Rev. B* **47**, 5485 (1993); C. T. White and T. N. Todorov, *Nature (London)* **323**, 240 (1998).
  - <sup>25</sup>M. Damnjanović, I. Milošević, T. Vuković, and J. Maultzsch, *J. Phys. A* **36**, 5707 (2003).
  - <sup>26</sup>O. E. Alon, *Phys. Rev. B* **63**, 201403 (2001).
  - <sup>27</sup>M. Damnjanović, E. Dobardžić, and I. Milošević, *J. Phys. C* **16**, L505 (2004).
  - <sup>28</sup>R. A. Jishi, L. Venkataraman, M. S. Dresselhaus, and G. Dresselhaus, *Chem. Phys. Lett.* **209**, 77 (1993).
  - <sup>29</sup>A. M. Rao, E. Richter, S. Bandow, B. Chase, P. C. Eklund, K. A. Williams, S. Fang, K. R. Subbaswamy, M. Menon, A. Thess, R. E. Smalley, G. Dresselhaus, and M. S. Dresselhaus, *Science* **275**, 187 (1997).
  - <sup>30</sup>A. Kasuya, Y. Sasaki, Y. Saito, K. Tohji, and Y. Nishina, *Phys. Rev. Lett.* **78**, 4434 (1997).
  - <sup>31</sup>E. Richter and K. R. Subbaswamy, *Phys. Rev. Lett.* **79**, 2738 (1997).
  - <sup>32</sup>J. Kürti, G. Kresse, and H. Kuzmany, *Phys. Rev. B* **58**, R8869 (1998).
  - <sup>33</sup>S. Reich, C. Thomsen, and P. Ordejón, *Phys. Rev. B* **64**, 195416 (2001).
  - <sup>34</sup>A. Jorio, A. G. Souza Filho, G. Dresselhaus, M. S. Dresselhaus, A. K. Swan, M. S. Ünlü, B. B. Goldberg, M. A. Pimenta, J. H. Hafner, C. M. Lieber, and R. Saito, *Phys. Rev. B* **65**, 155412 (2002).
  - <sup>35</sup>J. Maultzsch, S. Reich, C. Thomsen, E. Dobardžić, I. Milošević, and M. Damnjanović, *Solid State Commun.* **121**, 471 (2002).
  - <sup>36</sup>Z. M. Li, Z. K. Tang, G. G. Siu, and I. Bozovic, *Appl. Phys. Lett.* **84**, 4101 (2004).
  - <sup>37</sup>Z. M. Li, H. J. Liu, J. T. Ye, C. T. Chan, and Z. K. Tang, *Appl. Phys. A: Mater. Sci. Process.* **78**, 1121 (2004).
  - <sup>38</sup>O. Dubay, G. Kresse, and H. Kuzmany, *Phys. Rev. Lett.* **88**, 235506 (2002).